Journal of Catalysis **211,** 1–5 (2002)
doi:10.1006/jcat.2002.3741

PRIORITY COMMUNICATION

Hydroxyl Groups on γ-Alumina Surfaces: A DFT Study

M. Digne,*,†,‡ P. Sautet,*,† P. Raybaud,‡,[1] P. Euzen,§ and H. Toulhoat#

*Laboratoire de Chimie Théorique et des Matériaux Hybrides, Ecole Normale Supérieure de Lyon, 46 allée d'Italie, 69364 Lyon Cedex 07, France; †Institut de Recherches sur la Catalyse, Centre National de la Recherche Scientifique, 2 avenue Albert Einstein, 69626 Villeurbanne Cedex, France; and ‡Division Chimie et Physico-Chimie Appliquées, §Division Cinétique et Catalyse, and #Direction Scientifique, Institut Français du Pétrole, 1-4 avenue de Bois-Préau, 92852 Rueil-Malmaison Cedex, France

Received June 7, 2002; revised June 29, 2002; accepted June 29, 2002

Despite numerous experimental studies devoted to the acid–base properties of γ-alumina, the precise nature of surface acid sites remains unsolved. Using density functional (DFT) calculations, we propose realistic models of γ-alumina (110) and (100) surfaces accounting for hydroxylation/dehydroxylation processes induced by temperature effects. The vibrational analysis, based on DFT calculations, leads to an accurate assignment of the OH stretching frequencies observed by infrared (IR) spectroscopy. The extension to chlorinated surfaces, which brings new insights into the understanding of the role of dopes, is also addressed.

Key Words: **γ-alumina; oxide surfaces; catalyst support; DFT calculations; hydroxyl group; infrared analysis; Brønsted acidity; surface chlorination.**

INTRODUCTION

There are many major industrial applications of γ-alumina (1, 2). It is used as a support for refining processes catalysts (hydrotreatment, reforming), as a cocatalyst for chemical reactions involving acidic functions (reforming, isomerization), and as a sorbent for gas dehydration processes. The control of the surface acid–base properties of γ-alumina is a fundamental aspect of the reactivity of the final catalyst as well as of preparation and synthesis steps. The nature of the surface sites governs the dispersion of the supported active phases and modifies the catalyst's acidic function, if doped by chlorine.

For these reasons, γ-alumina has been the subject of many experimental studies, such as temperature-programmed desorption (3), calorimetry measurements (4, 5), infrared (IR) spectroscopy (6–12), and nuclear magnetic resonance (NMR) (12–14). The two latter techniques brought insights into the physical characterization of surface hydroxyl groups. In particular, the high-frequency region of the IR spectra (above 3000 cm^{-1}) contains up to seven bands corresponding to the stretching frequencies of OH groups (11). According to the complexity of this spectrum, the features of which may also depend on the sample preparation conditions, OH band assignment remains controversial. In the spirit of the work of Tsyganenko (6) and Morterra *et al.* (7), Knözinger and Ratnasamy (8) proposed an empirical model, which is still the most widely used. According to this approach, five bands are assigned to different types of OH groups exhibiting distinct "net electric charges," depending on the number of aluminum neighbors in the first oxygen sphere and on the aluminum coordination. More recently Busca *et al.* (9) proposed an interpretation of the IR spectrum closer to that of Morterra *et al.* (7), putting forward significant discrepancies with the Knözinger assignment. The available models suffer from serious limitations, mainly due to the crude description of ideal γ-alumina surfaces, neglecting surface hydroxylation/dehydroxylation processes induced by temperature effects.

As a consequence, to address fundamental, and still open, questions related to the γ-alumina acido–basicity, there is a clear need for establishing improved and rational models by undertaking modern *ab initio* simulations. The challenge of the present communication is to revisit the assignment of γ-alumina IR bands in the region of hydroxyl groups stretching frequencies, on the basis of realistic models of surfaces derived from first-principle calculations. For this purpose, the temperature-dependent hydroxyl coverages of these structural models have been determined with Gibbs free energy calculations. As an example of the important implications for industrial catalysts preparations by impregnation/anionic exchange, we further address the chlorination of γ-alumina.

METHODS

Calculations are based on the plane wave DFT method, with the nonlocal exchange-correlation functional

[1] To whom correspondence should be addressed. Fax: +33 1 47 52 70 58. E-mail: pascal.raybaud@ifp.fr.

0021-9517/02 $35.00

proposed by Perdew *et al.* (15), as implemented in the Vienna *Ab Initio* Simulation Package (VASP) (16, 17). Vanderbilt's ultrasoft pseudopotentials are used for describing ion–electron interactions, with an energy cutoff of 300 eV. The geometry optimization is performed for all the structures. For the integration in the reciprocal space, a convergence better than 1 meV/(Al_2O_3 unit) is obtained for a **k**-point grid's fineness of 0.05 $Å^{-1}$.

The stretching frequencies of OH groups are predicted, using a harmonic approach based on the numerical calculation of the Hessian matrix. Due to the high anharmonicity of OH bonds, these values are corrected by an anharmonicity term of 80 cm^{-1}, as calculated by Raybaud *et al.* (25) for similar OH groups of boehmite γ-AlOOH.

The model used for constructing γ-alumina surfaces is taken from our recent DFT study investigating the dehydration of boehmite into γ-Al_2O_3 (18). This cell model, containing 8 Al_2O_3 units, offers the best compromise. Within system sizes tractable by *ab initio* simulations, it reproduces the main experimental characteristics of bulk γ-alumina (19): the oxygen atoms sublattice is a face-centered cubic one, 25% of aluminum atoms are in tetrahedral sites, and the simulated XRD diagram is consistent with the experimental one. The hydrogen spinel structure HAl_5O_8 recently proposed in Ref. (20) was not chosen, due to its thermal instability, as shown by Wolverton and Hass (21), and Digne *et al.* (22). The choice of crystallographic surfaces is based on the morphology of γ-alumina nanoparticles. The (110) surface corresponds to a rectangular oxygen atom sublattice in the spinel description and exhibits the predominant area between 70 and 83% (23, 24). The (100) surface corresponding to a square oxygen atoms sublattice is less abundant and accounts for 17%, according to Ref. (23). The (111) surface can be exposed, too, but its importance depends on the synthesis conditions (24). The present study will focus on the (110) and (100) surfaces.

The hydroxylation/dehydroxylation process of the two (*hkl*)-oriented surfaces is described by the equilibrium

$$\text{Surface}_{hkl} + n_{\text{ads}}H_2O(\text{gas}) \rightleftharpoons [\text{Surface}_{hkl}, n_{\text{ads}}H_2O], \quad [1]$$

where n_{ads} stands for the number of adsorbed water molecules. The Gibbs free energy variation associated with Eq. [1] at a given temperature, T, and water pressure, p, is

$$\Delta_r G_{hkl} = G(\text{surf}_{hkl} + n_{\text{ads}}H_2O) - G(\text{surf}_{hkl}) - n_{\text{ads}}\mu_{H_2O}, \quad [2]$$

where μ_{H_2O} is the chemical potential of water. For the condensed phases, we can neglect the entropic and pV terms, as well as thermal variations of internal energies. Within these approximations, Eq. [2] is rewritten at atmospheric pressure,

$$\Delta_r G_{hkl} = n_{\text{ads}}\Delta_r g_{hkl} \quad [3]$$

$$= n_{\text{ads}}[\Delta e_{hkl} + Ts(T) - (h(T) - e(0))], \quad [4]$$

where s, h, and e are the entropy, enthalpy, and internal energy of water and Δe_{hkl} is the adsorption energy at 0 K of n_{ads} water molecules on the (*hkl*) surface expressed per H_2O molecules. An expression of the surface energy Γ_{hkl}, as a function of n_{ads} and T, is finally given by

$$\Gamma_{hkl} = \Gamma^0_{hkl} + \theta_{hkl}\frac{\Delta_r g_{hkl}}{2}, \quad [5]$$

where θ_{hkl} stands for the hydroxyl surface coverage and is equal to $2n_{\text{ads}}/A_{hkl}$, A_{hkl} is the geometric area of the (*hkl*) surface, and Γ^0 is the surface energy of a fully dehydrated surface ($\theta_{hkl} = 0$), referenced to the bulk Gibbs free energy. For a given θ_{hkl}, the lowest value for Δe_{hkl} represents the stable configuration among all the possible adsorption sites and adsorption modes of the n_{ads} water molecules. Allowing θ_{hkl} to vary, the lowest value of Γ_{hkl} corresponds to the stable hydroxylation state of the surface for a given temperature. As a consequence, according to Eq. [5], we determine unambiguously the concentration and types of

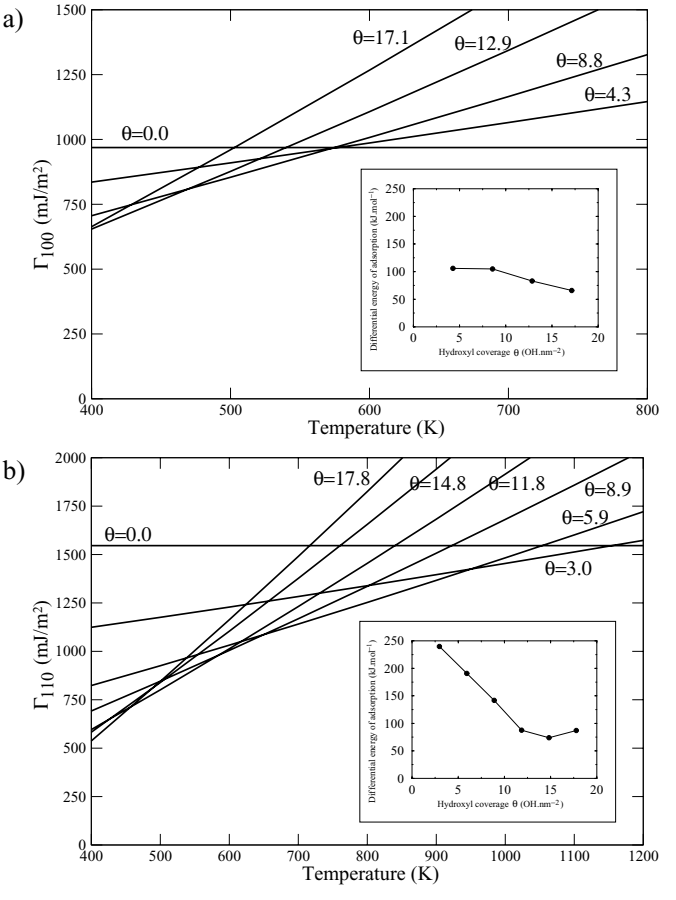

FIG. 1. Surface energy of (a) γ-Al_2O_3 (100) and (b) γ-Al_2O_3 (110) surfaces as a function of temperature for different hydroxyl coverages (θ in $OH \cdot nm^{-2}$). Insets represent the differential energy of adsorption as a function of θ. The differential energy of adsorption is the difference between the adsorption energies of $n+1$ water molecules and n water molecules, expressed per water molecule.

hydroxyl groups as well as coordinated unsaturated aluminum sites present on the surface as a function of temperature (see Fig. 1).

RESULTS AND DISCUSSION

Hydration as a Function of Temperature

For $\theta_{100} = 0$, the relaxation of the (100) surface shows that only onefold unsaturated octahedral aluminum atoms are stable (Al_V in Fig. 2a). The (110) surface exhibits two kinds of unsaturated aluminum surface sites: 75% of twofold unsaturated octahedral aluminum atoms and 25% of onefold unsaturated tetrahedral aluminum atoms (Al_{IV} and Al_{III}, respectively, in Fig. 2b). The surface energies are $\Gamma^0_{100} = 970\ \text{mJ} \cdot \text{m}^{-2}$ and $\Gamma^0_{110} = 1545\ \text{mJ} \cdot \text{m}^{-2}$. The energetics of the hydration process are significantly different for the two surfaces. As depicted in the inset to Fig. 1a), the differential energy of adsorption (see caption of Fig. 1 for the definition) on the (100) surface slightly decreases with an increase in hydroxyl coverage from 106 $\text{kJ} \cdot \text{mol}^{-1}$ for a dissociative chemisorption at low coverage ($\theta_{100} = 4.3\ \text{OH} \cdot \text{nm}^{-2}$) to 66 $\text{kJ} \cdot \text{mol}^{-1}$ for one H-bonded water molecule adsorption, leading to one monolayer of adsorbed water molecules ($\theta_{100} = 17.1\ \text{OH} \cdot \text{nm}^{-2}$). This small variation is due to the fact that local environments are very similar for all Al_V sites, presenting comparable Lewis acidity strengths. For the (110) surface, the differential energy of adsorption strongly decreases with hydroxyl coverage (see inset to Fig. 1b). For the dissociative chemisorption at $\theta_{110} = 3.0\ \text{OH} \cdot \text{nm}^{-2}$ on the Al_{III} site, the differential energy is 240 $\text{kJ} \cdot \text{mol}^{-1}$ due to the strong Lewis acidity of unsaturated Al_{III} sites. The adsorption leading to one monolayer of adsorbed water molecules ($\theta_{110} = 17.8\ \text{OH} \cdot \text{nm}^{-2}$) is a dissociative chemisorption on Al_V sites with a differential adsorption energy of 87 $\text{kJ} \cdot \text{mol}^{-1}$. This strong decrease in the adsorption energy on the predominant (110) surface is in good agreement with calorimetric measurements evaluating the differential energy at about 190 $\text{kJ} \cdot \text{mol}^{-1}$ for $\theta = 1.0\ \text{OH} \cdot \text{nm}^{-2}$ and at 66 $\text{kJ} \cdot \text{mol}^{-1}$ for $\theta = 8.0\ \text{OH} \cdot \text{nm}^{-2}$ (4).

Regarding morphology effects, it should be recalled that γ-alumina is obtained by a calcination process of boehmite at 700 K through a topotactic transformation. Thus, the morphology of γ-alumina nanoparticles corresponds not to the thermodynamic equilibrium (as given by the surface energies reported in Fig. 1) but to the inherited morphology of boehmite particles. This explains why, according to Beaufils and Barbaux (23), the predominantly exposed surface is the (110) basal plane, inherited from the (010) and (100) boehmite surfaces. The low-area (100) and (111) edge planes are thus inherited from the (001) and (101) boehmite edge surfaces.

Concerning the thermal stability, the surface energy diagrams of Fig. 1 show that the (100) surface is completely dehydrated above 600 K, whereas on the (110) surface, hydroxyl groups remain stable even at high temperature. We deduce that the concentration of OH surface sites for standard γ-alumina nanoparticles (using the morphology determined in Ref. (23)) drops from 12.0 $\text{OH} \cdot \text{nm}^{-2}$ at 450 K to 4.9 $\text{OH} \cdot \text{nm}^{-2}$ at 880 K. These estimates are semiquantitatively consistent with NMR experimental

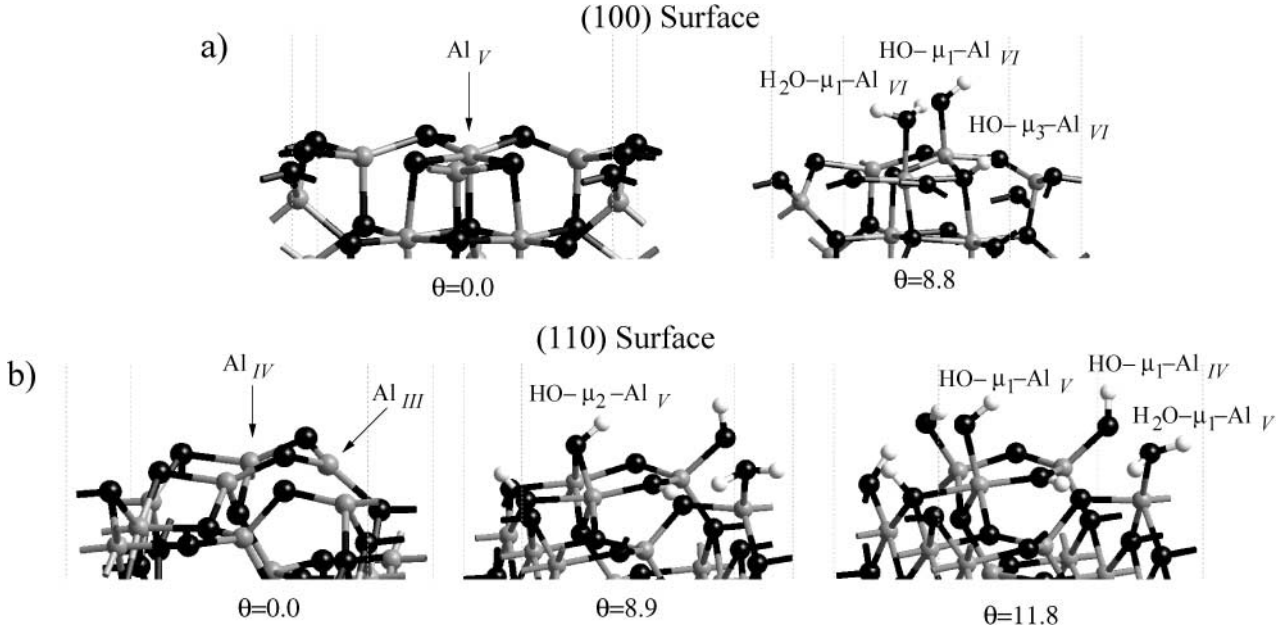

FIG. 2. Relaxed configurations of (a) γ-Al_2O_3 (100) and (b) γ-Al_2O_3 (110) surfaces for different hydroxyl coverages (θ in $\text{OH} \cdot \text{nm}^{-2}$). The most relevant surface sites are quoted. Al_n stands for aluminum atoms surrounded by n oxygen atoms, and HO–μ_m for OH groups linked to m aluminum atoms. (Black balls) Oxygen atoms; (gray balls) aluminum atoms; (white balls) hydrogen atoms.

measurements revealing a decrease from 8.2 to 2.1 $OH \cdot nm^{-2}$ for a similar range of temperatures (13). At the same time, the calculated concentrations of OH-free Al surface sites increases from 0.4 to 3.8 $Al \cdot nm^{-2}$ when increasing temperature. At high temperature, the (100) surface will be predominantly covered by unsaturated surface Al sites, i.e., Lewis sites.

Vibrational Analysis

As the number of surface OH groups depends on the pretreatment temperature, we consider surface hydroxylation corresponding to a standard outgassing at 573 K. For this temperature, the calculated hydroxyl coverages are $\theta_{110} = 11.8$ and $\theta_{100} = 8.8$ $OH \cdot nm^{-2}$. The calculated stretching frequencies are reported in Table 1.

The main OH bands observed in the high-frequency region of the IR spectra correspond to OH species exhibiting distinct local environments. As proposed by Knözinger and Ratnasamy (8), the OH stretching frequency depends on the number of Al neighbors in the first coordination sphere of the oxygen atom and on the coordination number of Al itself. However, our assignment diverges from the Knözinger's model on the following points. The two highest frequencies, at 3800 cm^{-1} (calculated at 3842 cm^{-1}) and 3775 cm^{-1} (calculated at 3777 cm^{-1}), correspond to terminal groups (μ_1) attached to Al_{IV} and Al_{VI}, respectively. Calculations on boehmite surfaces (25) already revealed the same attribution. The band at 3730 cm^{-1} (calculated at 3736 cm^{-1}) is attributed to a terminal group (μ_1) attached to Al_V sites located on the (110) surface. The existence of fivefold-coordinated aluminum atoms has been shown by MAS NMR ^{27}Al (26). Our simulations demonstrate clearly that bridged OH groups (μ_2) present on the (110) surface exhibit unambiguously lower frequencies at about 3690 cm^{-1} (calculated at 3707 cm^{-1}), which is also consistent with the calculated frequency of bridged OH groups on boehmite (010) (25) and with the recent proposal of Busca *et al.* (9). Finally, tribridged species (μ_3) of the (100) surface are responsible for the OH band observed at 3590 cm^{-1} (calculated at 3589 cm^{-1}), as proposed in (9). As a corollary, we notice that the OH region of the IR spectrum cannot be captured by considering only OH bridging Al atom pairs, as in (27). Regarding the four highest band assignments, Busca proposed recently to introduce the effect of vacancies for justifying the four observed μ_1 configurations. Our simulation recovers three frequencies attributed to μ_1-Al_{IV} (calculated at 3842 cm^{-1}), μ_1-Al_{VI} (calculated at 3777 cm^{-1}), and μ_1-Al_V (calculated at 3736 cm^{-1}) species found on distinct surfaces. Thus, it seems to be an effect of surface orientation more than of vacancy. Although this point should be further confirmed by simulations on the (111) surface, the band at 3740–3745 cm^{-1}, not yet identified in our work, might be attributed to OH species located on the (111) surface. Indeed, a similar band at 3742 cm^{-1} (11) is observed on α-alumina, the predominant (0001) surface of which exhibits the same type of surface sites as γ-Al_2O_3(111), resulting from the alternate stacking of aluminum and oxygen atoms planes.

The effect of hydrogen bonding is also rendered by our simulations. For instance, the μ_1-Al_{IV} group of the (110) surfaces involved in an hydrogen bond exhibits a frequency shifted down to 3206 cm^{-1}. It should be also noted that two high frequencies are predicted for the molecularly absorbed H_2O at 3616 and 3717 cm^{-1}. These groups are responsible for the broadening of the spectral features observed on γ-Al_2O_3.

A final and crucial learning of these results is that the different types of OH bands can be expressed as a function of the surface orientations. As a consequence, one can expect the IR spectrum to be sensitive to the morphology of the boehmite precursor.

Chlorination of Surfaces

Starting from the previous well-defined hydrated surfaces, the surface chlorination may occur by addition of gas-phase hydrogen chloride, HCl, leading to the substitution

TABLE 1

Vibrational Stretching Frequencies of Surface Hydroxyl Groups Obtained for $\theta = 11.8$ and 8.8 $OH \cdot nm^{-2}$ for the (110) and (100) Surfaces, Respectively, and Substitution Energy by a Chlorine Atom[a]

Site	Surface	d(OH) (Å)	$\omega_{cal.}$ (cm^{-1})	$\omega_{exp.}$ (cm^{-1})	Knözinger's assignment	Δ_rH(Cl) ($kJ \cdot mol$)
HO–μ_1-Al_{IV}	(110)	0.984	3842	3785–3800	HO–μ_1-Al_{VI}	+19
HO–μ_1-Al_{VI}	(100)	0.988	3777	3760–3780	HO–μ_1-Al_{IV}	+2
HO–μ_1-Al_V	(110)	0.988	3736	3730–3735	HO–μ_2-(Al_{VI}, Al_{IV})	−4
HO–μ_2-Al_V[b]	(110)	0.991	3707	3690–3710	HO–μ_3	+29
HO–μ_3-Al_{VI}	(100)	0.997	3589	3590–3650	H bonded	+95
HO–μ_1-Al_{IV}[c]	(110)	1.019	3206			+42
H_2O–μ_1-Al_{VI}	(100)	0.992/1.096	3717			+12
H_2O–μ_1-Al_V	(110)	0.998/1.093	3616			+31

[a] The frequencies are corrected by an anharmonicity term of 80 cm^{-1} (see also Ref. 25).
[b] OH group stable at lower hydroxyl coverage ($\theta = 8.9$ $OH \cdot nm^2$).
[c] OH group involved in a hydrogen bond.

of surface OH groups; i.e.,

$$-\mathrm{Al}_n(\mathrm{OH})- + \mathrm{HCl(gas)} \rightleftharpoons -\mathrm{Al}_n(\mathrm{Cl})- + \mathrm{H_2O(gas)}, \quad [6]$$

where n is the coordination of the surface OH (or Cl) species. The enthalpy variations related to Eq. [6], $\Delta_r H(\mathrm{Cl})$, are given in Table 1.

In most cases, the substitution of OH by Cl is an endothermic process. For the μ_2 and μ_3 groups, the endothermicity can be explained by steric constraints: the optimal Al–Cl distance (2.2–2.4 Å) is larger than the optimal Al–OH one (1.8–2.0 Å). As a consequence, it is difficult to simultaneously accommodate two- or threefold-coordinated Cl atoms without strong local deformations which are energetically unfavorable (Table 1). The case of μ_1-OH groups is different: the substitution by a Cl atom implies that the optimal geometry is matched for the μ_1-$\mathrm{Al_{VI}}$ and μ_1-$\mathrm{Al_V}$ groups on (100) and (110) surfaces, respectively, with Al–Cl distance of 2.38 and 2.22 Å, respectively. Both processes are close to be athermic: $\Delta_r H(\mathrm{Cl}) = +2$ and $-4\ \mathrm{kJ \cdot mol}$, respectively. The μ_1-$\mathrm{Al_{IV}}$ group of the (110) surface reveals a more complex situation. The corresponding substitution is slightly endothermic ($\Delta_r H(\mathrm{Cl}) = +19\ \mathrm{kJ \cdot mol}$), which is explained by the complete modification of the surface hydrogen bonds network. As the O–H $\cdots$ Cl bond is weaker than the O–H $\cdots$ O bond, the substitution of OH groups by Cl atoms in the surface hydrogen network is less stable. At a lower hydroxyl coverage ($\theta = 3.0\ \mathrm{OH \cdot nm^{-2}}$), for which the hydrogen bonds network is removed, the same process becomes slightly exothermic ($\Delta_r H(\mathrm{Cl}) = -6\ \mathrm{kJ \cdot mol}$). This phenomenon is rather general and also occurs for the μ_1-$\mathrm{Al_{VI}}$ position, where the substitution energy decreases from $+2$ to $-4\ \mathrm{kJ \cdot mol^{-1}}$ when θ decreases from 8.8 to 4.3 $\mathrm{OH \cdot nm^{-2}}$. Finally, the substitution of the molecularly chemisorbed H_2O by HCl is an endothermic process ($\Delta_r H(\mathrm{Cl}) = +12$ and $+31\ \mathrm{kJ \cdot mol}$) and leads to the dissociation of the HCl molecule. As a conclusion, upon chlorination, the energetically most favorable chlorine substitution occurs on HO–μ_1 groups. This result is in good agreement with IR observations (12, 28). Vigué *et al.* (28) reported that the three highest bands, at 3787, 3778, and 3722 $\mathrm{cm^{-1}}$, disappear whereas the bands at 3675 and 3596 $\mathrm{cm^{-1}}$ remain present after chlorination.

CONCLUSIONS

Using DFT simulations, realistic models of γ-alumina (110) and (100) surfaces were proposed for the first time, taking into account temperature effects on the hydroxyl surface coverage. The calculation of surface OH stretching frequencies allowed a precise assignment of experimental frequencies, as a function of the local environment of the OH groups, overcoming the limits of empirical models. Furthermore, it was demonstrated that these frequencies are dependent on the exposed surfaces, i.e., the morphology of the γ-alumina, inherited from the boehmite precursor after calcination. A first study of the surface chlorination was proposed, consistent with the vibrational analysis. The correct surface density and vibrational properties of hydroxyl groups clearly show that the selected models are valid representations of the active surface of γ-alumina catalyst. Therefore, for this complex and important material in catalysis, the results of the present communication open new opportunities to predict catalytic activity of the support and to investigate interactions between the active phase and the support surfaces, governing the dispersion of the active phases.

REFERENCES

1. Ertl, G., Knözinger, H., and Weitkamp, J., "The Handbook of Heterogeneous Catalysis." Wiley–VCH, Weinheim, 1997.
2. Euzen, P., Raybaud, P., Krokidis, X., Toulhoat, H., Le Loarer, J.-L., Jolivet, J.-P., and Froidefond, C., *in* "Handbook of Porous Materials" (F. Schüth, K. Sing, and J. Weitkamp, Eds.), Chap. 4, 7, 9, pp. 1591–1677. Wiley-VCH, Weinheim, 2002.
3. Abello, M. C., Velasco, A. P., Gorriz, O. F., and Rivarola, J. B., *Appl. Catal. A* **129**, 93 (1995).
4. Hendriksen, B. A., Pearce, D. R., and Rudham, R., *J. Catal.* **24**, 82 (1972).
5. Auroux, A., Muscas, M., Coster, D. J., and Fripiat, J. J., *Catal. Lett.* **28**, 179 (1994).
6. Tsyganenko, A. A., and Filimonov, V. N., *J. Mol. Struct.* **19**, 579 (1973).
7. Morterra, C., Ghiotti, G., Boccuzzi, F., and Coluccia, S., *J. Catal.* **51**, 299 (1978).
8. Knözinger, H., and Ratnasamy, P., *Catal. Rev.–Sci. Eng.* **17**, 31 (1978).
9. Busca, G., Lorenzelli, V., Sanchez Escribano, V., and Guidetti, R., *J. Catal.* **131**, 167 (1991).
10. Mohammed Saad, A. B., Ivano, V. A., Lavalley, J. C., Nortier, P., and Luck, F., *Appl. Catal.* **94**, 71 (1993).
11. Morterra, C., and Magnacca, G., *Catal. Today* **27**, 497 (1996).
12. Guillaume, D., Gautier, S., Alario, F., and Devès, J. M., *Oil Gas Sci. Technol. Rev. IFP* **54**(4), 537 (1999).
13. Hietala, J., Root, A., and Knuuttila, P., *J. Catal.* **150**, 46 (1994).
14. Sang, H., Chu, H. Y., and Lunsford, J. H., *Catal. Lett.* **26**, 235 (1994).
15. Perdew, J. P., Chevary, J. A., Vosko, S. H., Jackson, K. A., Pedersen, M. R., Singh, D. J., and Frolhais, C., *Phys. Rev. B* **46**, 6671 (1992).
16. Kresse, G., and Furthmüller, J., *Comput. Mater. Sci.* **6**, 15 (1996).
17. Kresse, G., and Furthmüller, J., *Phys. Rev. B* **54**, 11961 (1996).
18. Krokidis, X., Raybaud, P., Gobichon, A.-E., Rebours, B., Euzen, P., and Toulhoat, H., *J. Phys. Chem. B* **105**, 5121 (2001).
19. Zhou, R. S., and Snyder, R. L., *Acta Crystallogr. B* **47**, 617 (1991).
20. Sohlberg, K., Pennycook, S. J., and Pantelides, S. T., *J. Am. Chem. Soc.* **121**, 7493 (1999).
21. Wolverton, C., and Hass, K. C., *Phys. Rev. B* **63**, 24102 (2001).
22. Digne, M., Sautet, P., Raybaud, P., Toulhoat, H., and Artacho, E., *J. Phys. Chem. B* **106**, 5155 (2002).
23. Beaufils, J. P., and Barbaux, Y., *J. Chim. Phys.* **78**, 347 (1981).
24. Nortier, P., Fourre, P., Mohammed Saad, A. B., Saur, O., and Lavalley, J. C., *Appl. Catal.* **61**, 141 (1990).
25. Raybaud, P., Digne, M., Iftimie, R., Wellens, W., Euzen, P., and Toulhoat, H., *J. Catal.* **201**, 236 (2001).
26. Chen, F. R., Davis, J. G., and Fripiat, J. J., *J. Catal.* **133**, 263 (1992).
27. Fripiat, J. J., Alvarez, L. J., Sánchez, J. S., Morales, E. M., Saniger, J. M., and Sánchez, N. A., *Appl. Catal.* **215**, 91 (2001).
28. Vigué, H., Quintard, P., Merle-Méjean, T., and Lorenzelli, V., *J. Eur. Ceram. Soc.* **18**, 305 (1998).